Effect of Temperature and Humidity on Dielectric Properties of Thermally Sprayed Alumina Coatings

Minna Niittymäki and **Kari Lahti**
Tampere University of Technology
Electrical Energy Engineering
P.O. Box 692
FI-33101 Tampere, Finland

Tomi Suhonen and **Jarkko Metsäjoki**
VTT Technical Research Centre of Finland
P.O. Box 1000
FI-02044 Espoo, Finland

ABSTRACT

Breakdown strength, DC resistivity, permittivity and loss of thermally sprayed alumina coatings were studied at various temperatures and relative humidities. The studied coatings were sprayed by utilizing three different spray techniques: flame, high-velocity oxygen fuel (HVOF) and plasma spraying. Breakdown behavior of HVOF sprayed alumina were studied up to very high temperatures (800 °C). At 20–180°C, no significant trend could be seen in the breakdown strength of HVOF and plasma sprayed alumina coatings. The breakdown strength of alumina coatings decreased gradually from 300 to 800 °C reaching a value which was only 14% of the breakdown strength measured at 20 °C/RH 20%. Increasing humidity (from 20 to 90%) decreased the DC resistivity of the alumina coatings five orders of magnitude. Correspondingly, permittivity and losses increased with the humidity; in most cases with a notable contribution due to DC conduction. The material behavior may be linked to the microstructure of coatings consisting of amorphous and crystalline regions with interfaces in between. Moreover, the alumina coatings exhibited notable amount of highly hygroscopic γ-phase which also affected the moisture sensitivity of the coatings.

Index Terms — **Alumina, aluminum oxide, thermally sprayed ceramic coating, flame spray, HVOF, plasma spray, dielectric breakdown, resistivity, conductivity, permittivity, dielectric losses**

1 INTRODUCTION

ALUMINA (Al_2O_3) is a widely used electrical insulation material in high temperature applications since it exhibits high hardness and refractory nature [1]. Thermal spraying is an effective and rather low cost method to produce a protective/insulating layer for demanding conditions such as thermal barrier coating in gas turbine components, protective insulation layer in aero-engine parts or in fuel cells [2, 3]. In the thermal spraying process, the raw alumina is typically in powder form but it can also be used in rod form [2–4]. During spraying, thermal energy is generated either by chemical (combustion) or electrical (plasma or arc) methods in order to melt and accelerate the ceramic powder particles towards the substrate [2, 3]. The molten particles form droplets which hit on the substrate (e.g. steel plate) or on the coating surface forming a coating consisting of thin layers of lamellae (called splats) [2, 3]. In particular, the lower surfaces of the splats cool down faster than the internal parts.

Manuscript received on 3 July 2017, in final form 1 February 2018, accepted 28 February 2018. Corresponding author: M. Niittymäki.

Due to this, the surfaces are normally more amorphous, while the internal parts are typically crystalline [3, 5]. In addition to the splats, the coating exhibits some unmelted powder particles, voids and often also some cracks which can be formed during cooling [1–3]. If long perpendicular cracks are formed, the breakdown strength of a thermally sprayed ceramic coating can decrease significantly as noticed in our previous study on $MgAl_2O_4$ coating [6].

Previous studies of the dielectric properties of thermally sprayed alumina coatings are mostly focused on the breakdown strength at room temperature. However, the effect of high temperature on the breakdown strength of alumina coatings is not studied although one relevant application for alumina coatings is solid oxide fuel cells which have very high operating temperatures (500–800 °C) [7]. Thus, one aim of this paper is to study the breakdown strength of alumina coatings at 120–800 °C. In addition, the breakdown strength is studied at the temperatures of 20–60 °C at various humidities in order to distinguish the possible effect on humidity.

The alumina coatings have a special lamellar microstructure, which differs significantly from sintered bulk alumina, and due to this direct comparison between the dielectric properties of these two is not worthwhile. Furthermore, the sintered alumina and alumina powder utilized in thermal spraying consist of thermodynamically stable α-Al_2O_3 as the main crystalline phase but due to the rapid solidification during the spraying [8] the alumina coatings exhibit metastable γ-phases as a main phase [9-13]. This γ-Al_2O_3 is highly hygroscopic [3, 14] which can be one reason for the significant increase of dielectric constants and losses of the coatings at high humidity [11, 15, 16]. However, the high amount of γ-phase in alumina coating cannot only explain the moisture sensitivity since the DC resistivity of $MgAl_2O_4$ coatings, which have stable crystalline phases, decreased several orders of magnitude with increasing humidity in [6, 12]. Thus, it should be emphasized that the special microstructure together with the hygroscopic nature can explain the moisture sensitive nature of the alumina coatings. However, the effect of humidity and temperature on the DC resistivity, permittivity and loss of thermally sprayed alumina coatings is not comprehensively studied. Due to this, together with the breakdown study the other aim of this paper is study the effect of temperature (20–60 °C) and humidity (20–90%) on the DC resistivity, permittivity and losses of thermally sprayed alumina coatings.

1.1 BACKGROUND

In this paper, the studied alumina coatings are deposited by utilizing three different spraying processes which are flame spraying, high-velocity oxygen fuel (HVOF) spraying, and atmospheric air plasma spraying (APS). The main differences between these techniques are flame temperature and powder particle velocity. In flame and HVOF spraying, the flame temperature is ~3000 °C [1, 3] while in the plasma spraying the temperature is >15000 °C [1, 2]. The powder particle velocities in flame, HVOF and plasma spraying are 30–120 m/s [1, 3], ~700–800 m/s [1, 17] and 100–300 m/s [1, 13], respectively. In particular, the high powder particle velocity improves the coating properties which can be seen in HVOF sprayed coatings as well-adhered and dense structures [1, 3]. However, numerous and complex processing parameters affect the coating properties and microstructure [4]. According to Kotlan *et al.* [13], increasing the spray distance in plasma spraying decreased the dielectric breakdown strength of alumina coating. However, increasing the spray distance had decreasing effect on the particle velocity and temperature [13], and thus it is difficult to distinguish exactly the effect of processing parameters on the dielectric properties.

The studies on the dielectric properties of thermally sprayed Al_2O_3 coatings are mainly focused on the dielectric breakdown strength. The DC breakdown strength of plasma sprayed alumina coatings has been reported to be 10–20 V/μm [11], 17–36 V/μm [18] and 22–23 V/μm [12] at room temperature conditions. Slightly higher DC breakdown strength is typically obtained for HVOF sprayed alumina: 22–34 V/μm [12], 20–32 V/μm [14] and 32 V/μm [19]. The AC breakdown strength of HVOF alumina coating was 29 V_{peak}/μm in our previous study [19]. The AC breakdown strength of plasma sprayed alumina coatings have been reported to be 13.5–16.6 V/μm [13], 6–17 V/μm [18] and 20–115 V/μm [5]. However, in [5] the breakdown measurements were performed in insulating oil. In our previous studies [19], the breakdown strength of HVOF sprayed alumina coating increased significantly in oil immersion in comparison to the breakdown strength obtained without oil since the thermally sprayed ceramic coatings are typically quite porous and sensitive to the moisture and liquids.

In comparison to the alumina coatings, sintered alumina exhibits typically dense and fully crystalline structure. Thus, utilization of insulation oil in breakdown voltage measurements has not been observed to affect the breakdown strength of sintered alumina [20–27]. However, the DC breakdown strength of sintered alumina can be at similar or higher level with the alumina coatings, being 90–150 V/μm [20], 30–130 V/μm [28], and 26–96 V/μm [25]. AC breakdown strength of sintered alumina is at a very similar level with the ceramic coatings since it was 31.6 V/μm [21], 15–34 V/μm [27], 22 V/μm [22], 13–15 V/μm [23], 19–25 V/μm [24], and 10–42 V/μm [26]. It should be noted that the thicknesses of the sintered alumina are typically higher than those of the coatings.

Typically, sintered alumina has higher DC resistivity (>10^{12} Ωm) [27] but the DC resistivity of thermally sprayed alumina coating can vary from 10^6 to 10^{11} Ωm [11, 12, 29]. Our previous studies [30–34] have shown that DC resistivity of thermally sprayed Al_2O_3 and $MgAl_2O_4$ coatings can be at the level of ~10^{12} Ωm at the electric fields below 1 V/μm but at higher electric fields the resistivity decreases several decades indicating a strong non-ohmic conductivity. In addition, the DC resistivity of the Al_2O_3 and $MgAl_2O_4$ coatings have been found to decrease several decades when the relative humidity increased [6, 12] which can be linked to moisture sensitive nature of the coatings.

Interestingly, notable differences in dielectric constant has not been reported. The dielectric constant of sintered alumina was 9 at 1 MHz [22, 27] and 7 at 1 kHz [25], while for plasma sprayed alumina it was 6–8 [11] and 11–23 [15] at 1 kHz, and for HVOF alumina 6–8 [35] at 10 kHz. However, the measuring frequencies are quite high and the microstructural differences between bulk and coating cannot be seen as clearly as they may be noticed in the DC conductivity and in the slow charging phenomena at lower frequencies. However, the dielectric constant of plasma sprayed alumina increased with humidity which was explained by the hygroscopic nature of the alumina coatings due to the high amount of metastable γ-phase instead the stable α-phase [15, 16].

1.2 THEORETICAL CONSIDERATIONS

Compared to typical insulating materials, the dielectric behavior of thermally sprayed ceramic coatings is remarkably different. Due to the manufacturing process, the coatings exhibit layered structure which consists of splats with clear interfaces in between (see Figure 1). As it was shown in [5], [33], amorphous and crystalline regions exist in the splats. These regions most probably have different conductivities as it was discussed in our previous studies in [33] where it was shown that the conduction mechanism of the coatings differ from the SCLC mechanism known for Al_2O_3 [22, 36]. A suggested conduction mechanism for the coatings in [33]

satisfies the measured non-linear conduction behavior and is based on the microstructural and phase differences of the coatings. Different conductivities in the different regions will lead the non-uniform field distribution and further, when the highly stressed regions turn into dominating SCLC conduction, the other regions still have ohmic conduction, resulting in the measured behavior.

Based on above, it may be hypothesized that the microstructure full of interfaces and splat volumes with presumably varying conductivities tend to enhance the interfacial type of polarization mechanisms at low frequencies, at least in cases with highest resistivity. On the other hand, at the same time the conductivity of the coatings may be remarkably high, which tend to limit and prevent the charging phenomena. When the DC conductivity is high, the conductivity σ will notably contribute to the imaginary part of the complex permittivity (ε_r*) [37]. It can be defined as:

$$\varepsilon_r^* = \varepsilon_r' - j\left(\varepsilon_r'' + \frac{\sigma}{\omega\varepsilon_0}\right) \quad (1)$$

where ε_r' is the is real part of the permittivity, ε_r'' is the loss term due to polarization, σ is DC conductivity, ω is the angular frequency, and ε_0 is vacuum permittivity [37]. Any dielectric measurement result always includes both loss components, caused by both polarization and conduction.

2 EXPERIMENTAL

2.1 MATERIAL CHARACTERIZATION

Three different Al_2O_3 materials were sprayed by HVOF, plasma or flame spray methods. In HVOF process, the coatings were deposited from fused high purity Al_2O_3 powder (99.9 wt %, Praxair). In plasma spraying process, another fused high purity Al_2O_3 powder (99.25 wt%, Saint-Gobain) was utilized. In the flame spray process, the Al_2O_3 was in a cord form (99.7 wt%, Saint-Gobain). All the coatings were sprayed on stainless steel substrates (100 × 100 × 2.5 mm). Before the spraying, the substrates were grit-blasted to ensure better adhesion between the substrate and the ceramic coating.

Breakdown voltage measurements for HVOF coatings were also made at high temperatures (200–800 °C). Since alumina and steel have different thermal expansion coefficients, which can cause problems at high temperatures, 80 µm thick bond coatings (NiCrAlY, H.C. Starck) were HVOF sprayed on the substrates before HVOF spraying the alumina powder (99.9 wt%, Praxair). The bond coat was found to have no significant effect on the breakdown strength of alumina coatings.

Figure 1 presents the cross-section images of the studied coatings. As it can be seen from the figure, all the coatings exhibit porous nature and lamellar structure. The porosities of the coatings were determined by analyzing cross-sectional micrographs taken by several different microscopy techniques, see Table 1. The porosities of Plasma coating defined from SEM images are at a higher level than those of HVOF coating which is attributable to the higher particle velocity in the HVOF process [2, 3]. The spraying process of Flexicord samples differs from the HVOF and plasma processes which can explain the higher porosities of Flexicord.

Sample thicknesses were measured with magnetic measuring device (Elcometer 456B) from the electrode areas (Ø=11 mm or Ø=50 mm depending on the test). The average thicknesses and standard deviations are listed in Table 1 (10 parallel measurements from the 50 mm electrode area). In addition, the coating thicknesses were also determined from cross-section images taken by optical microscope (Table 1). The standard deviations of the thicknesses are quite high which is partly due to the grit blasting of the coating substrate and consequently uneven lower surfaces of the coatings. In addition, the spraying process itself does not produce fully smooth coatings, which also partly explain the thickness deviation.

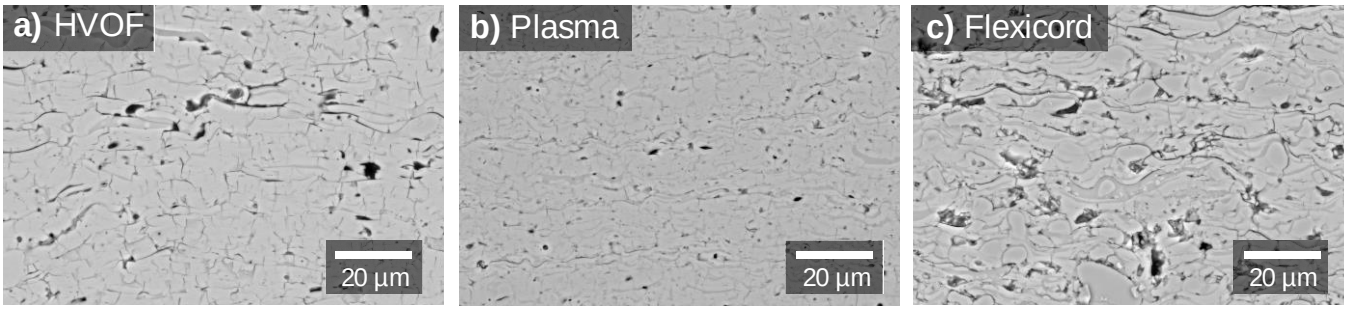

Figure 1. SEM/BSE cross-sectional images of the studied coatings at 1000× magnification (a–c). Black image regions correspond to void type imperfections, while in general, the light grey regions indicate crystalline material and the slightly darker color correspond to amorphous regions. Mainly in Flexicord image also unmelted particle regions can be seen.

Table 1. Raw material info of the studied coatings. The porosities of the coatings were defined from cross-sectional images taken by either optical microscope (OM, 320× magnification) and scanning electron microscope (SEM, 1000× magnification) using secondary electron detector (SE) and backscattered electron detector (BSE). Thicknesses of the coatings were determined by using cross-section images and utilizing magnetic measuring device.

Sample	Powder composition	Porosity (%)			Thickness (µm)		
		OM	SEM/SE	SEM/BSE	From cross-section image	From magnetic measurement	SD
HVOF	commercial Al_2O_3 (fused powder)	1.4	1.4	1.4	333	307	6.1
Plasma	commercial Al_2O_3 (fused powder)	2.3	2.4	3.6	245	271	11.4
Flexicord	commercial Al_2O_3 (cord)	2.7	3.8	4.8	235	225	4.4

2.2 DIELECTRIC CHARACTERIZATION

2.2.1 Sample preparation and measurement conditions

For DC resistivity and permittivity measurements, a round electrode (Ø=50 mm) was painted on the sample surface using a special silver paint (SPI High Purity Silver paint). In addition, a shield electrode was painted around the measuring electrode to prevent possible surface currents. For DC breakdown voltage measurements performed at the temperatures of 20–180 °C, smaller silver painted electrodes (Ø=11 mm) were prepared. Our previous study indicated that the silver paint does not penetrate into the coating [19]. After painting the electrodes, the samples were first dried at 120 °C for two hours followed by conditioning in a climate room at 20 °C/RH 20% for at least 12 h before the measurements. At 200–800 °C, the breakdown voltage measurements of HVOF coating were made without any embedded electrodes on the sample surface.

At 20–60 °C, the measurements were performed in a climate room where the temperature and relative humidity were controlled. The detailed measurement conditions are given in Table 2. The breakdown measurements for all coating types were made at 120 and 180 °C in a custom made oven. In addition, the breakdown behavior of HVOF sprayed alumina coating was also studied at the temperatures of 200, 300, 350, 400, 600 and 800 °C in a high temperature oven.

The coating samples were stabilized for three hours at the measurement conditions in the climate room before the resistivity, permittivity or breakdown measurements. In all the high temperature measurements, the coatings were placed into the oven at room temperature and the temperature was slowly increased to the set value. For the breakdown measurements at 120 and 180 °C, the heating times required for the samples to stabilize to set temperature were carefully determined prior to actual breakdown measurements. At 120 °C the stabilization period was one hour and at 180 °C it was two hours. At the high temperatures (200–800 °C), the temperature was increased with a ramp of 25 °C/min to the set point. When the steel substrate reached the set temperature, an hour was waited until the first breakdown measurement was started. After the measurements, the oven was switched off and the samples were left in the oven to slowly cool down to ~20 °C.

2.2.2 DC breakdown strength

DC breakdown voltage measurements were performed by utilizing linearly increased DC voltage (ramp rate of 100 V/s throughout the test). The voltage source control and data recording was performed using LabVIEW-based software. The voltage source was Spellman SL1200 (U_{max}=20 kV) and the voltage was measured using a resistive voltage divider (Spellman HVD-100-1, divider ratio 10000:1) [19].

Table 2. Measurement temperatures and relative humidities and the corresponding absolute humidities for resistivity and permittivity measurements. The breakdown measurement conditions are bolded.

Temperature (°C)	RH (%)	Absolute humidity (g/m³)
20	**20**	**3.5**
20	**45**	**7.8**
20	70	12.2
20	90	15.6
40	**20**	**10.3**
40	**45**	**23.1**
40	70	35.9
60	20	26.1
60	**45**	**58.7**
60	70	91.3

At 20–180 °C, a stainless steel rod electrode (Ø=11mm, edge rounding 1 mm) was placed on top of the silver painted area on the coating sample while the stainless steel substrate of the sample acted as the other electrode. In order to avoid surface flashovers at the highest test voltages at 20–60 °C, a plastic cylinder with an O-ring seal was clamped on the coating surface around the measuring electrode (Ø=11 mm) to extend the surface distance over the solid insulation. For high temperature measurements (200–800 °C), a nickel based rod electrode (Ø=9 mm) was placed on the sample surface while the substrate acted as the other electrode.

Dielectric breakdown strength (DBS) of a coating was calculated by dividing the breakdown voltage by the corresponding coating thickness at the painted electrode (Ø=11 mm) location. In the high temperature measurements (200–800 °C), the thickness was measured near the breakdown point after the measurement.

2.2.3 DC resistivity

Resistivity measurements were made using Keithley 6517B electrometer and a sample holder where the sample with substrate and silver painted electrode was placed in between two stainless steel electrodes (Ø=50 mm). The measuring electric field varied from 0.1 V/µm to 2.5 V/µm. The test voltage was maintained for a period of 300 s at each voltage step. Typically, the DC resistivity is determined from a stabilized current value (i.e. resistive current) but the current of the coatings did not reach a fully stabilized level at every applied field. However, the resistivity was defined from the average current value in the end of the measurement period. All the measuring arrangements were in accordance with the standard IEC 60093.

2.2.4 Relative permittivity and losses

Relative permittivity and losses of the material were studied by utilizing an insulation diagnosis analyzer device (IDA 200, U_{max}=200 V_{peak}) using the same sample holder as in the resistivity measurements. During the measurements, a sinusoidal voltage with varying frequency was applied over the sample. The measuring electric field strength was 0.3 V_{peak}/µm for all the coatings. All the test arrangements were performed in accordance with the IEC standard 60250.

The complex impedance of a sample was calculated from the measured test voltage and the current through a sample which was expressed by IDA device as the equivalent parallel RC circuit model. The real part of the relative permittivity (ε_r') is defined as:

$$\mathrm{Re}\left\{\varepsilon_r^*\right\} = \varepsilon_r' = \frac{C_p}{C_0} - \frac{C_e}{C_0} \qquad (2)$$

where C_p is measured parallel capacitance of the equivalent circuit. C_0 is the so-called geometric capacitance of the test sample (vacuum in place of the insulation) and ω is the angular frequency. The edge field correction (C_e) was not used since the shield electrode was utilized in the measurements. As indicated by Eq. 1, conductivity of a material will also contribute to the relative permittivity ($|\varepsilon_r^*|$).

However, in this paper ε_r' values are reported, which in authors' opinion better reflect the dielectric behavior of the materials.

Imaginary part of the relative permittivity indicates the total losses of a material, both polarization and conduction losses. It can be defined as:

$$\mathrm{Im}\left\{\varepsilon_r^*\right\} = \varepsilon_r'' + \frac{\sigma}{\omega\varepsilon_0} = \frac{1}{\omega R_p C_0} \quad (3)$$

where R_p is the parallel resistance of the equivalent circuit. In this paper, the total loss contribution is expressed. The conductivity related component can be estimated by using the measured conductivities but since the conductivity is shown to be dependent on several factors (e.g. field), an exact determination of the loss components would require more detailed studies. However, at the driest conditions the conductivity component is negligible (e.g. ~0.3% for HVOF at 20 °C/RH 20%) but it is totally dominating at the highest absolute humidities, see Figure 6.

3 RESULTS AND DISCUSSION

3.1 DC BREAKDOWN STRENGTH

The DC breakdown strengths (BDS) of the studied coatings at each conditions are presented in Table 3, where the results are based on 10–15 parallel breakdown measurements. In addition, Figure 2 shows the BDS of the coatings at 20, 60 and 180 °C. The highest BDS is noticed for HVOF at all the ambient conditions and the lowest one for Flexicord. The deviation between parallel samples was the highest for Plasma coatings, as indicated by the lowest Weibull β values in Table 3.

At 20–40 °C, the BDS of HVOF alumina remains at very similar level (α=34–39 V/µm) but at 60 °C/RH 45% it decreased slightly (α=28 V/µm). However, similar decrease cannot be seen for Plasma and Flexicord since at 20–60 °C the BDS for Plasma is 17–21 V/µm and for Flexicord 12–18 V/µm. The obtained breakdown strengths are at similar level with breakdown strengths of HVOF and plasma sprayed alumina coatings reported in the literature [5, 12–14, 18] as well as with our previous studies [6, 19, 32, 33]. Although the higher absolute humidity conditions seemed to decrease the BDS of HVOF alumina, similar effect is not seen for other coatings and it may be concluded that humidity did not directly affect the breakdown strength.

At 120 and 180 °C, the breakdown strength of HVOF does not change in comparison to the 20 °C/RH 20% results (α=34 V/µm at 120 °C and 35 V/µm at 180 °C). However, at 120 °C the BDS of Plasma is obviously higher (α= 27 V/µm) than at

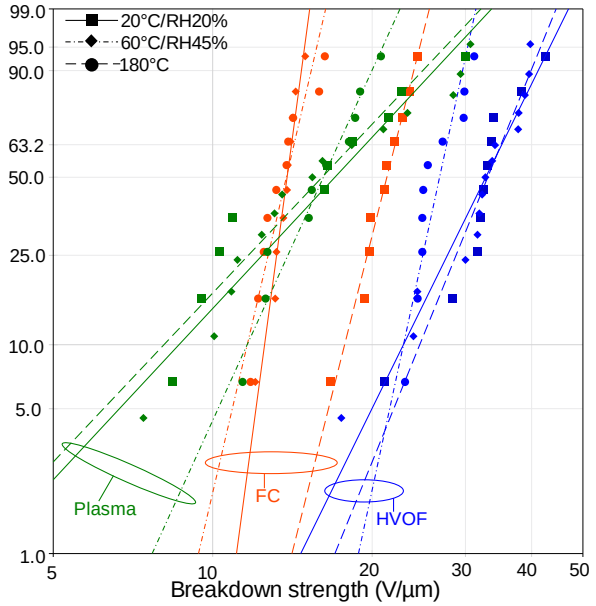

Figure 2. DC breakdown strenghts of the studied coatings at 20°C, 60°C and 180°C (FC is Flexicord).

20–60 °C but at 180 °C the BDS (α=18 V/µm) is again at a similar level with the low temperature results. It should be noted that the deviation in breakdown data of Plasma is very high (low β values in Table 3).

The breakdown strength of Flexicord is 22 V/µm at 120 and 180 °C which is higher than the BDS at the low temperatures. It may be speculated especially for Flexicord that at the higher temperatures (120 and 180 °C), moisture is partially escaped from the porous coating, and thus the BDS increases compared to 20–60 °C results. Pawlowski [11] noticed that the dielectric constant of plasma sprayed alumina decreased after a long (48 h) period at 120 °C which was linked to the hygroscopic nature of the coatings which enables the moisture to penetrate into the coating easily. In this study, although the samples were in oven for a shorter period (1–2 hours) than in [11], the heat treatment most probably removed part of the moisture from the porous coating. This can explain the higher breakdown strengths of Flexicord at 120 and 180 °C.

Pawlowski [11] also noticed that high porosity decreased the breakdown strength of the plasma sprayed alumina coating. Toma *et al.* [12] made similar observation since HVOF sprayed alumina coating had a lower porosity and correspondingly a higher BDS than a plasma sprayed alumina coating. Our own previous studies have shown that high porosity of HVOF sprayed MgO-Al_2O_3 coatings (as indicated

Table 3. The breakdown fields of the studied coatings at the breakdown probabilities of 10%, 63.2% and 90% at 20°C–180°C and Weibull β. The statistical analysis of the breakdown data was performed using Weibull++® software and the least-square regression method was used in parameter estimation. The goodness of the fit results can be expressed by correlation coefficient, λ. The closer to 1 λ is, the better the fit is. λ was 0.91–0.97 for HVOF, 0.93–0.98 for Plasma and 0.93–0.98 for Flexicord.

	HVOF				Plasma				Flexicord			
	E_{bd} (V/µm)			β	E_{bd} (V/µm)			β	E_{bd} (V/µm)			β
	10 %	α, 63.2 %	90 %		10 %	α, 63.2 %	90 %		10 %	α, 63.2 %	90 %	
20°C/RH 20%	22.9	35.1	41.2	5.3	8.6	19.4	26.2	2.8	12.5	14.1	14.7	19.3
20°C/RH 45%	29.5	39.2	43.5	7.9	8.7	18.7	24.8	3.0	11.8	13.8	14.7	14.3
40°C/RH 20%	27.2	38.7	44.1	6.4	17.2	21.2	22.9	10.8	16.3	17.6	18.1	30.2
40°C/RH 45%	29.0	35.6	38.5	10.9	8.8	16.8	21.3	3.5	10.7	12.4	13.1	15.4
60°C/RH 45%	22.9	27.6	29.6	12.0	11.6	17.3	20.0	5.7	11.6	14.2	15.3	11.1
120°C	24.1	33.9	38.5	6.6	18.8	27.0	30.9	6.2	17.7	21.7	23.4	11.0
180°C	24.6	35.0	39.9	6.4	8.1	18.4	24.9	2.7	17.7	22.1	24.0	10.3

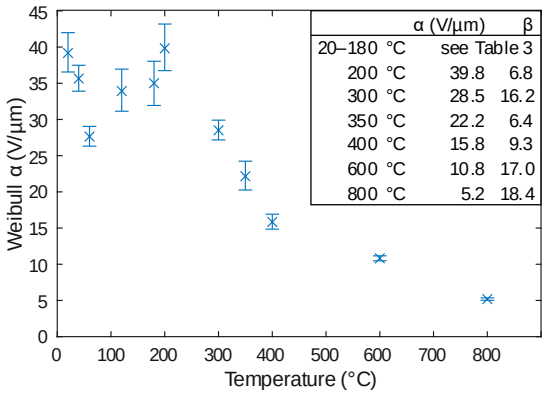

Figure 3. BDS of HVOF alumina as a function of temperature. The error bars represent the 90% confidence bounds. The relative humidity was 45% in 20°C, 40°C and 60°C results.

by relatively high gas permeability) decreased the breakdown strength [6], although for some of the HVOF alumina coatings similar decrease was not noticed [33]. Although the effect of porosity on the breakdown strength is not always so straightforward, in this study the most porous alumina coating (Flexicord) had also the lowest BDS while the lowest porosity alumina coating (HVOF) exhibited the highest BDS.

Since the ceramic coating may be used also at notably higher temperatures than 180 °C, the breakdown measurements were extended to higher temperatures (200–800 °C). Figure 3 presents the breakdown strength of the HVOF coating as a function of temperature. The BDS is at quite similar level from 20 to 200 °C although the deviation between the parallel samples is quite large in many cases. Interestingly, the deviation between parallel samples is remarkably lower at higher temperatures (above 350 °C) which can be seen as a high β in Figure 3. Above 300 °C the breakdown strength starts to decrease reaching the value of 5.2 V/µm at 800 °C which is 14% of the BDS at 20 °C/RH 20%. Yoshimura and Bowen [20] made almost similar observation since the breakdown strength of polycrystalline alumina decreased gradually from room temperature (90–100 V/µm) to 900 °C (~25 V/µm). Above 900 °C, the BDS of alumina decreased at much higher rate reaching 2 V/µm at 1400 °C [20].

3.2 DC RESISTIVITY

Figure 4 presents the DC resistivity of the coatings as a function of electric field at all the studied ambient conditions. At 20 °C/RH 20%, the DC resistivities of all the coatings are at the level of ~10^{12} Ωm from 0.1 to 0.5 V/µm. Above 0.5 V/µm, the resistivities start to decrease gradually indicating a non-ohmic behavior which has also been observed in our previous studies [30, 31, 33, 34]. In [33], a detailed analysis of DC conduction mechanisms up to breakdown fields was made for HVOF and plasma sprayed Al_2O_3 coatings and for several HVOF sprayed Al_2O_3-MgO coatings. It was speculated [33], that the conductivity of the coatings follows only partly the space charge limited conduction (SCLC) mechanism unlike the sintered bulk alumina [22], [36]. The microstructure of the ceramic coating, which consists of amorphous and crystalline regions as well as voids and unmelted particles, can be thought as an insulation system in which the conductivity of the amorphous regions is most probably higher than that of the crystalline regions. The differences in the conductivities and the resulting non-

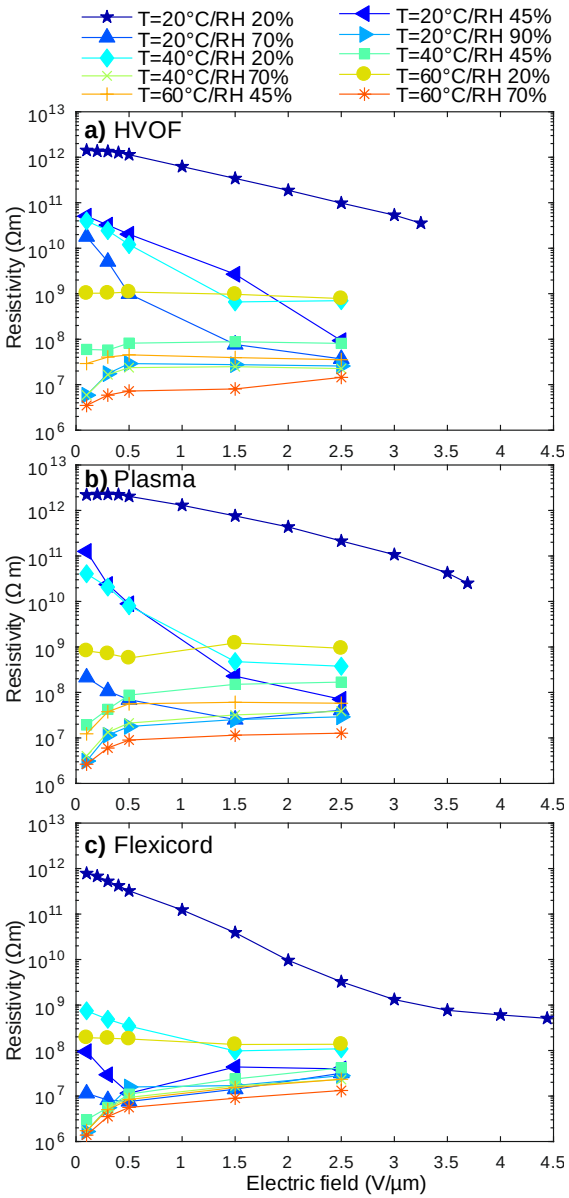

Figure 4. DC resistivity of the coatings as a function of electric field.

uniform electric field distribution are most probably the reasons why the coatings exhibit non-linear conductivity already at rather low electric fields in comparison to crystalline bulk alumina [33].

When the humidity and temperature increase above 20 °C/RH 20%, the non-ohmic conductivity cannot be seen for Flexicord (Figure 4). However, it can be noticed for HVOF and Plasma at 20 °C/RH 45% and at 40 °C/RH 20% but not at higher temperatures or humidities. It can be speculated that the conductivity caused by observed moisture most probably overrun the non-ohmic behavior of the coatings at high absolute humidities.

The resistivities of the coatings at the electric field of 0.3 V/µm are listed in Table 4. It can be noticed that Flexicord has evidently lower resistivity at all conditions in comparison to HVOF and Plasma which exhibit very similar resistivities. The differences of DC resistivities at various conditions between the coating types may be linked to their different microstructural features since the spraying parameters (e.g. flame temperature, particle velocity) affect the coating microstructure. The interfaces, thicknesses of the amorphous and crystalline layers, etc. differ between the coating types

Table 4. The DC resistivity at the electric field of 0.3 V/μm for the studied coatings as well as the real part of permittivity (ε_r') at frequency of 50 Hz and the imaginary part of permittivity ($\varepsilon_r''+\sigma/\omega\varepsilon_0$) indicating total losses at 50 Hz and 1 kHz.

		HVOF				Plasma				Flexicord			
T (°C)	RH (%)	ρ (Ωm)	ε_r' (50Hz)	$Im\{\varepsilon_r^*\}$ (50Hz)	$Im\{\varepsilon_r^*\}$ (1kHz)	ρ (Ωm)	ε_r' (50Hz)	$Im\{\varepsilon_r^*\}$ (50Hz)	$Im\{\varepsilon_r^*\}$ (1kHz)	ρ (Ωm)	ε_r' (50Hz)	$Im\{\varepsilon_r^*\}$ (50Hz)	$Im\{\varepsilon_r^*\}$ (1kHz)
20	20	1.3×10^{12}	11.3	3.8	0.7	2.3×10^{12}	12.9	4.5	0.7	5.3×10^{11}	13.0	5.4	1.1
20	45	3.2×10^{10}	25.0	21.8	4.1	2.4×10^{10}	26.6	22.5	4.1	2.9×10^{7}	33.5	51.8	7.2
20	70	5.1×10^{9}	44.5	60.2	9.3	1.1×10^{8}	40.0	216.9	17.4	8.2×10^{6}	42.7	92.5	10.8
20	90	1.8×10^{7}	53.2	253.6	22.6	1.2×10^{7}	68.8	997.7	60.6	5.6×10^{6}	54.3	216.3	18.1
40	20	2.4×10^{10}	14.8	6.9	1.6	2.1×10^{10}	15.2	6.6	1.2	4.9×10^{8}	16.6	9.3	2.0
40	45	5.8×10^{7}	39.2	30.2	6.8	4.3×10^{7}	37.9	31.0	7.0	5.6×10^{6}	34.0	61.4	7.8
40	70	1.7×10^{7}	53.5	116.5	14.8	1.3×10^{7}	43.3	271.1	21.0	5.4×10^{6}	42.5	160.6	14.9
60	20	1.0×10^{9}	18.8	10.0	2.5	7.1×10^{8}	18.3	8.6	1.9	1.9×10^{8}	18.4	10.3	2.5
60	45	4.1×10^{7}	49.4	47.1	9.9	3.8×10^{7}	41.0	34.9	8.2	5.0×10^{6}	47.1	74.4	11.1
60	70	5.9×10^{6}	49.3	155.5	15.9	6.0×10^{6}	55.7	266.2	22.8	3.5×10^{6}	46.7	248.2	19.7

and these differences can partly explain the differences in the DC resistivities.

It may be speculated that porosity partly affects the DC resistivity since the highest porosity alumina coating (Flexicord) exhibits the lowest resistivities at all conditions while HVOF exhibits the highest resistivity and correspondingly the lowest porosity. Plasma has slightly lower resistivity and higher porosity than HVOF. Pawlowski [11] noticed that the most porous plasma sprayed alumina coating exhibited the lowest DC resistivity which is well in line with the results in this study. Also, the DC resistivities of plasma sprayed alumina coatings were 5×10^{9}–3×10^{12} Ωm in [11] which is comparable to the results obtained in this study.

As can be seen from Table 4, increasing the relative humidity from 20 to 90% decreased the DC resistivity of the studied coatings five orders of magnitude at 0.3 V/μm. Toma *et al.* made similar observation in [12] when increasing the relative humidity from 30 to 95% decreased the DC resistivity of HVOF sprayed alumina coating from 1×10^{11} Ωm to 3×10^{5} Ωm. For the plasma sprayed (APS) alumina coating the decrease was from 3×10^{11} to 2×10^{4} Ωm.

In our previous study [30], the DC resistivity of spinel ($MgAl_2O_4$) coatings deposited by HVOF, Plasma and Flexicord techniques were studied at 20–60 °C at RH 20% and 45%. When comparing the DC resistivities of the spinel coatings to the resistivity of alumina coatings in this study, the values are at very similar level at 20 °C/RH 20%. However, when the temperature or humidity was increased above 20 °C/RH 20%, the resistivities of these alumina coatings decreased more than those of spinel coatings in [30] although the porosities of the spinels coatings in [30] were slightly higher. It can be speculated that the alumina together with water forms to aluminum hydroxide which can have a decreasing effect on the resistivity of alumina coatings. According to Toma *et al.* [12], the HVOF and plasma sprayed spinel coatings exhibit higher resistivities at RH 30% and RH 90% in comparison to the alumina coatings. In our previous study [6], the DC resistivity of HVOF sprayed Al_2O_3-MgO coatings decreased correspondingly to the DC resistivities in here (five orders of magnitude) when the humidity increased from 20% to 90%. However, the DC resistivities of the Al_2O_3-MgO coatings [6] were at a higher level at 20 °C/RH 20% than the resistivities of Al_2O_3 coatings in here. It was also noticed in [6] that the high porosity (as indicated by relatively high gas permeability) did not affect the resistivity although the humidity increased from 20 to 90%.

As it was discussed in [12] and as the resistivity results indicate in this study, the thermally sprayed alumina coatings exhibit sensitivity to absorbed moisture due to the nature of the coating, the microstructure, and the phase composition. However, as indicated by the above analysis, it is very difficult to clearly distinguish between exact effects of various microstructural or other details on the resistivity with increasing humidity, -only above like speculations may be made. However, it can be seen that all the coatings can absorb notable amount of moisture which can significantly decrease the resistivity, seemingly stabilizing to the range of 10^{7}–10^{8} Ωm. At the same time, the resistivity seems to turn from originally field dependent behavior to linear behavior.

3.3 RELATIVE PERMITTIVITY AND LOSSES

Figure 5 and Figure 6 present the relative permittivities and the total loss contributions of the studied Al_2O_3 coatings as a function of frequency at 20–60°C. As can be seen from the figures, at the low frequencies (below 1 Hz) the permittivities and the losses increase 3–5 orders of magnitude, indicating the notable conduction at increased humidities, as seen also in the resistivity results. At higher frequencies, the increase is much lower. However, it shall be remembered that the given permittivity values are the real parts of the complex permittivity (see Eq. 1) and do not thus include the loss related component, only the real polarizability related component. It can be speculated that main part of the increased permittivity is most probably originating from water content (H_2O: $\varepsilon_r\approx80$ at 20°C). Interestingly, the permittivity increases at lower frequencies also at driest conditions which may be due to the hypothesized interfacial polarization due to the coating microstructure with varying conductivities.

The increase in the real part of relative permittivity is well in line with the literature since Brown *et al.* noticed [15] that the dielectric constant of plasma sprayed alumina coating increased from 8.3 to 9.8 at 100 kHz when the relative humidity increased from 0% to 95%. In this study, the dielectric constant of plasma sprayed alumina coating increased from 9.8 to 30.6 at 1 kHz when the humidity increased from 20 to 90%. In our previous studies [30], the dielectric constants of HVOF, plasma and Flexicord sprayed $MgAl_2O_4$ coatings were found to increase with increasing temperature (20 to 60°C) when relative humidity was either 20 or 45%. The dielectric constants of the spinel coatings in [30] were at lower level than those of alumina coatings in this

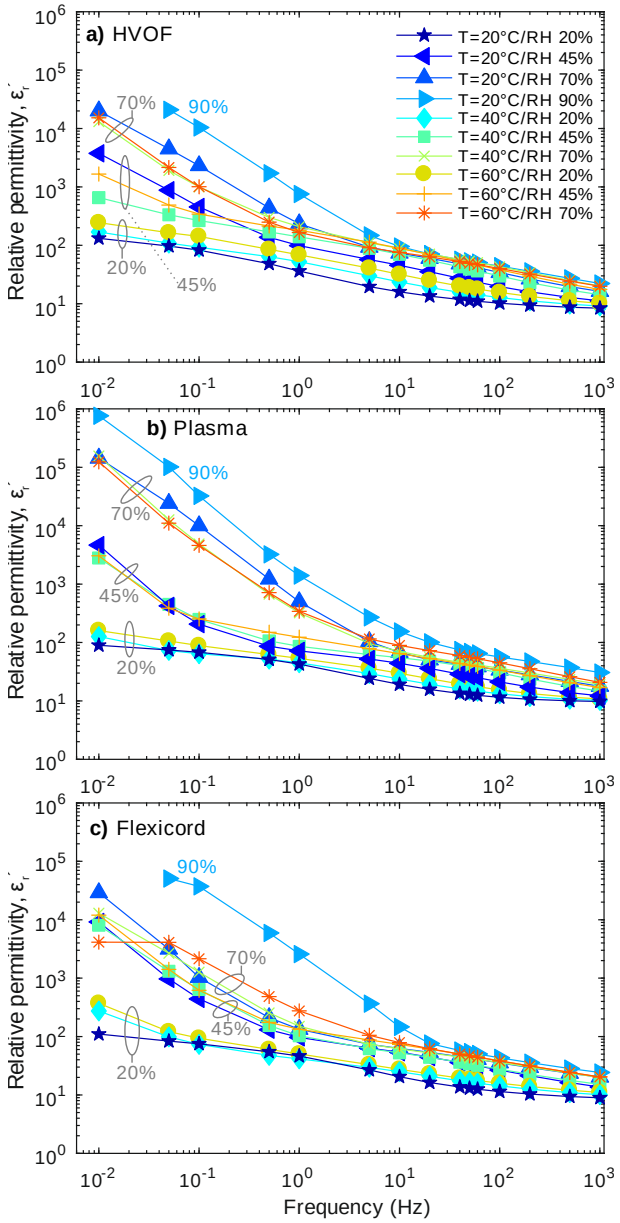

Figure 5. Relative permittivity (indicated as Re{ε_r*}) as a function frequency when the measuring electric field was 0.3 V_{peak}/µm. In RH 90% measurements, the high losses caused measurement problems and due to this the permittivity data at lowest frequencies are missing.

study. This is well in line with the DC resistivity results since the spinel coatings exhibited also higher DC resistivities in [30] than the alumina coatings in this study. In general, the lamellar microstructure with interfaces and regions of different dielectric properties enhance the permittivity of the coatings.

At 20 °C/RH 20% at the frequency of 1 kHz, the dielectric constants of HVOF, Plasma and Flexicord alumina are 8.4, 9.8 and 8.9, respectively. In [35], the dielectric constant of HVOF alumina coatings varied from 5.9 to 8.2 at 10 kHz which is quite well in line with the results obtained in this study. Brown *et al*. noticed [15] that the dielectric constant of plasma alumina coating was 11–23 at 1 kHz when the highest value was obtained for the coating which exhibited the lowest powder particle size. Correspondingly, the lowest dielectric constant was obtained for the highest particle size coating. These values are quite well in line with the real part of relative permittivity of Plasma at 20 °C/RH 45% and 20 °C/RH 70% where the permittivity was 12.2 and 17.8, respectively. Pawlowski reported in [11] that the dielectric constant of plasma sprayed alumina coatings was 6–8 at 1 kHz, which is slightly lower than reported in here. The differences in the dielectric constants can be partly explained by the different sample preparation since in [15] the coating samples were baked for 13 hours at 135 °C and in [11] for 1–3 days at 120°C while in here the samples were heat-treated in 120 °C for 2 hours. Longer baking time removes more completely moisture from a porous coating which can be seen as lower dielectric constant.

It should be noted that the measuring voltage was 1 V_{rms} in [11] while in this study the measuring voltage depends on the coating thickness varying from 57 V_{rms} to 69 V_{rms} corresponding to the electric field of 0.3 V_{peak}/µm. Although the measuring field might affect the relative permittivity, we noticed in [32] that at the frequency of 100 Hz the real part of relative permittivity of HVOF alumina and spinel coatings was not dependent on the measuring electric field (0.1–5 V/µm). However, at 0.1 Hz small increase in the real part of relative permittivity can be seen for some of the samples when the electric field was above 0.5 V/µm which is similar non-linear behavior as noticed for DC conductivity in [32].

As it can be seen from Figure 6, the losses increase with increasing humidity. The effect of increasing humidity on the losses at various temperatures can be seen in detail in Figure 7 where the losses are presented at the frequency of 50 Hz. It needs to be emphasized that the presented values indicate total measured losses including the contributions of both DC conductivity and polarization (see Eq. 3). At high humidities, the DC conduction part of the losses is more dominant limiting and preventing the charging phenomena, which can be seen obviously in Figure 6. HVOF alumina coating has the lowest losses while the Flexicord exhibits the highest values, see Figure 7 and Table 4. This similar trend was also noticed in the DC resistivity results.

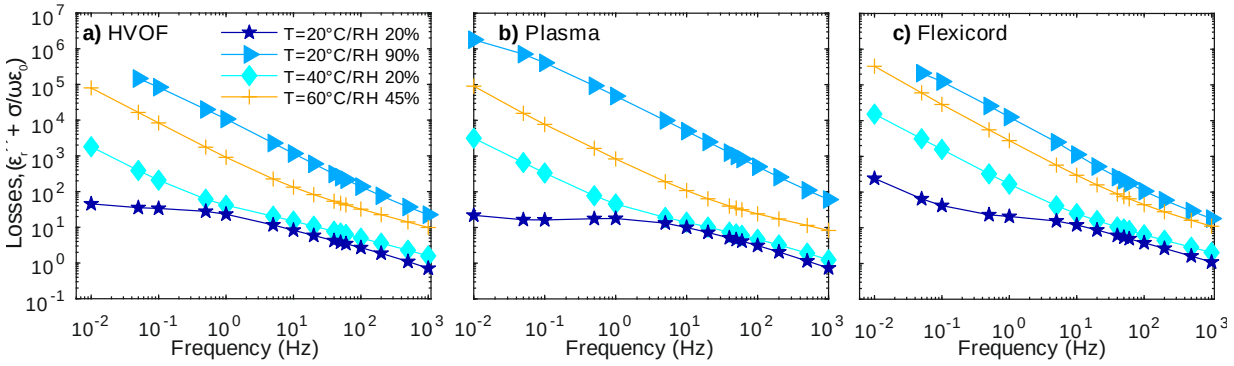

Figure 6. Losses (indicated as Im{ ε_r*}) as a function frequency when the measuring electric field was 0.3 V_{peak}/µm.

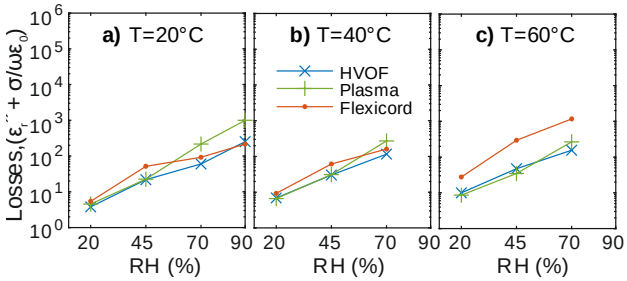

Figure 7. a)–c) The losses of the coatings at the frequency of 50 Hz.

3.4 FURTHER DISCUSSION

The results indicate that the dielectric properties of thermally sprayed alumina coatings clearly differ from that of bulk alumina, and thus lamellar microstructure and porosity most probably affect the dielectric properties. Furthermore, the properties of alumina change during thermal spraying process since varying amount of metastable γ-Al_2O_3, which is more hygroscopic than the stable α-Al_2O_3 [11, 12, 14], may form. Brown *et al.* [15] and Pawlowski [11] proposed that high dielectric constant of plasma sprayed alumina coating is related to high γ-Al_2O_3 content. Toma *et al.* [12] noticed that HVOF sprayed alumina coating had higher α-phase content than plasma alumina coating and correspondingly at high humidities (>RH 75%) the HVOF alumina coating had higher resistivity than plasma alumina but at low humidities (<RH 45%) the HVOF and plasma alumina exhibited similar resistivities. Anyhow, for both coating types the resistivity decreased approximately five orders of magnitude when the relative humidity increased from 30 to 95% [12] which is a similar decrease as obtained in this study. Toma *et al.* suggested in [14] that the higher DC resistivity of suspension HVOF alumina coating can be due to lower porosity and higher α-Al_2O_3 content in comparison to the conventional HVOF alumina coatings

However, Favre *et al.* [38] noticed that the DC resistivity of α-Al_2O_3 powder decreased approximately five orders of magnitude when the relative humidity increased from 20% to 80%. Thus, high γ-content of thermally sprayed alumina coatings cannot explain completely their sensitivity to the humidity. Although thermally sprayed spinel coatings exhibit more stable form also in coating [12, 15], their dielectric properties are also sensitive to the humidity [6, 12, 30, 39]. Thus, the nature of thermally sprayed ceramic coatings is moisture sensitive. If the operation temperatures of a thermally sprayed coatings are low enough, it is possible to impregnate a coating with an organic or inorganic sealant in order to make it more insensitive against the moisture penetration [40]. This also affects the dielectric properties of the impregnated coating.

4 CONCLUSIONS

Dielectric properties of thermally sprayed alumina coatings were studied at various conditions. It was found that spraying technique, temperature and humidity affected notably the dielectric properties. However, temperature had only a minor effect on the breakdown strength of the alumina coatings in the range of 20–180°C although the deviation in the breakdown data was quite high. The breakdown strength of alumina coatings decreased gradually from 300 to 800 °C reaching a value which was only 14% of the breakdown strength measured at 20 °C/RH 20%.

DC resistivity, permittivity and losses of the studied alumina coatings were at quite similar level at low temperatures and humidities. However, increasing the relative humidity from 20 to 90% decreased DC resistivity five orders of magnitude while AC losses increased correspondingly. In all coating types, permittivity increased at low frequencies also at dry conditions, possibly indicating interfacial type of polarization.

These major changes with humidity are attributable to the highly hygroscopic nature of the coatings, which, for alumina coatings, can partly be explained by the notable amount of metastable γ-phase. Moreover, the lamellar microstructure consisting of amorphous and crystalline regions with interfaces and voids in between can be speculated to enhance the moisture sensitive nature of the coatings.

In the potential applications for thermally sprayed ceramic insulations, the insulating layers are subjected to demanding conditions (e.g. high temperature, challenging geometries, mechanical or chemical stress, etc.). Thus, careful consideration of the effect of demanding conditions on dielectric properties of thermally sprayed ceramic coatings is of great importance in order to enable their reliable operation in final applications. Furthermore, it is necessary to evaluate the long-term ageing and degradation behavior of the coatings.

REFERENCES

[1] B. Basu and K. Balani, *Advanced Structural Ceramics*. Wiley-American Ceramic Society Inc, 2011.

[2] J. R. Davis, *Handbook of Thermal Spray Technology*. United States of America: ASM International, 2004.

[3] L. Pawlowski, *The Science and Engineering of Thermal Spray Coatings*, 2nd ed. Chichester, West Sussex, England: John Wiley & Sons Ltd, 2008.

[4] A. Piqué *et al.*, "Chapter 9 – Direct-Write Thermal Spraying of Multilayer Electronics and Sensor Structures," in *Direct-Write Technologies for Rapid Prototyping*, A. Pique and D. Chrisey, Eds. Academic Press, 2002, pp. 261–302.

[5] E. E. J. Young, E. Mateeva, J. J. Moore, B. Mishra, and M. Loch, "Low pressure plasma spray coatings," *Int. Conf. Metall. Coatings Thin Film.*, vol. 377–378, pp. 788–792, 2000.

[6] M. Niittymäki, I. Rytöluoto, K. Lahti, J. Metsäjoki, and T. Suhonen, "Role of microstructure in dielectric roperties of thermally sprayed ceramic coatings," in *IEEE International Conference on Dielectrics (ICD)*, 2016, pp. 1102–1105.

[7] N. H. Menzler, F. Tietz, S. Uhlenbruck, H. P. Buchkremer, and D. Stöver, "Materials and manufacturing technologies for solid oxide fuel cells," *J. Mater. Sci.*, vol. 45, no. 12, pp. 3109–3135, Feb. 2010.

[8] A. Kulkarni *et al.*, "Studies of the microstructure and properties of dense ceramic coatings produced by high-velocity oxygen-fuel combustion spraying," *Mater. Sci. Eng. A*, vol. 369, no. 1–2, pp. 124–137, Mar. 2004.

[9] R. McPherson, "Formation of metastable phases in flame- and plasma-prepared alumina," *J. Mater. Sci.*, vol. 8, no. 6, pp. 851–858, 1973.

[10] R. McPherson, "A review of microstructure and properties of plasma sprayed ceramic coatings," *Surf. Coatings Technol.*, vol. 39, pp. 173–181, 1989.

[11] L. Pawlowski, "The relationship between structure and dielectric properties in plasma-sprayed alumina coatings," *Surf. Coatings Technol.*, vol. 35, no. 3–4, pp. 285–298, 1988.

[12] F. L. Toma, S. Scheitz, L. M. Berger, V. Sauchuk, M. Kusnezoff, and S. Thiele, "Comparative study of the electrical properties and characteristics of thermally sprayed alumina and spinel coatings," *J. Therm. Spray Technol.*, vol. 20, no. 1–2, pp. 195–204, 2011.

[13] J. Kotlan, R. C. Seshadri, S. Sampath, P. Ctibor, Z. Pala, and R. Musalek, "On the dielectric strengths of atmospheric plasma sprayed Al_2O_3, Y_2O_3, ZrO_2–7% Y_2O_3 and (Ba,Sr)TiO_3 coatings," *Ceram. Int.*,

vol. 41, no. 9, pp. 11169–11176, Nov. 2015.
[14] F. L. Toma *et al.*, "Comparison of the microstructural characteristics and electrical properties of thermally sprayed Al_2O_3 coatings from aqueous suspensions and feedstock powders," *J. Therm. Spray Technol.*, vol. 21, no. 3–4, pp. 480–488, 2012.
[15] L. Brown, H. Herman, and R. K. MacCrone, "Plasma-sprayed insulated metal substrates," in *Proceedings of the Elevent International Thermal Spray Conference*, 1986, pp. 507–512.
[16] S. Sampath, "Thermal spray applications in electronics and sensors: past, present, and future," *J. Therm. Spray Technol.*, vol. 19, no. 5, pp. 921–949, Feb. 2010.
[17] S. Deshpande, A. Kulkarni, S. Sampath, and H. Herman, "Application of image analysis for characterization of porosity in thermal spray coatings and correlation with small angle neutron scattering," *Surf. Coatings Technol.*, vol. 187, no. 1, pp. 6–16, Oct. 2004.
[18] H. L. Filmer, J. Hochstrasser, A. R. . Nicoll, and S. Rangaswamy, "Plasma spray deposition of alumina-based ceramic coatings," *Am. Ceram. Soc. Bull.*, vol. 69, no. 12, pp. 1955–1958, 1990.
[19] M. Niittymäki, K. Lahti, T. Suhonen, and J. Metsäjoki, "Dielectric breakdown strength of thermally sprayed ceramic coatings: effects of different test arrangements," *J. Therm. Spray Technol.*, vol. 24, no. 3, pp. 542–551, Jan. 2015.
[20] M. Yoshimura and H. K. Bowen, "Electrical breakdown strength of alumina at high temperatures," *J. Am. Ceram. Soc.*, vol. 64, no. 7, pp. 404–410, 1981.
[21] I. O. Owate and R. Freer, "Ac breakdown characteristics of ceramic materials," *J. Appl. Phys.*, vol. 72, no. 6, pp. 2418–2422, 1992.
[22] F. Talbi, F. Lalam, and D. Malec, "DC conduction of Al_2O_3 under high electric field," *J. Phys. D. Appl. Phys.*, vol. 40, no. 12, pp. 3803–3806, 2007.
[23] L. Haddour, N. Mesrati, D. Goeuriot, and D. Tréheux, "Relationships between microstructure, mechanical and dielectric properties of different alumina materials," *J. Eur. Ceram. Soc.*, vol. 29, no. 13, pp. 2747–2756, Oct. 2009.
[24] D. Malec, V. Bley, F. Talbi, and F. Lalam, "Contribution to the understanding of the relationship between mechanical and dielectric strengths of alumina," *J. Eur. Ceram. Soc.*, vol. 30, no. 15, pp. 3117–3123, 2010.
[25] C. Neusel, H. Jelitto, D. Schmidt, R. Janssen, F. Felten, and G. A. Schneider, "Thickness-dependence of the breakdown strength: Analysis of the dielectric and mechanical failure," *J. Eur. Ceram. Soc.*, vol. 35, no. 1, pp. 113–123, Jan. 2015.
[26] F. Talbi, F. Lalam, and D. Malec, "Dielectric breakdown characteristics of alumina," in *Proceedings of the International Conference on Solid Dielectrics (ICSD)*, 2010, pp. 1–4.
[27] D. Malec, V. Bley, T. Lebey, F. Talbi, and F. Lalam, "Investigations on dielectric breakdown of ceramic materials," in *Annual Report Conference on Electrical Insulation and Dielectric Phenomena, 2005.*, 2005, pp. 63–66.
[28] C. Neusel and G. A. Schneider, "Size-dependence of the dielectric breakdown strength from nano- to millimeter scale," *J. Mech. Phys. Solids*, vol. 63, no. February, pp. 201–213, 2014.
[29] J. Luth, M. Cichosz, M. Lehmann, S. Hartmann, and F. Trenkle, "High velocity oxygen fuel sprayed insulation coatings for applications in high power electronics," in *Proceedings of the International Thermal Spray Conference*, 2015, pp. 1026–1030.
[30] M. Niittymäki, T. Suhonen, J. Metsäjoki, and K. Lahti, "Influence of humidity and temperature on the dielectric properties of thermally sprayed ceramic $MgAl_2O_4$ coatings," in *Annual Report Conference on Electrical Insulation and Dielectric Phenomena*, 2014, pp. 94–97.
[31] M. Niittymäki, T. Suhonen, J. Metsäjoki, and K. Lahti, "DC dielectric breakdown behavior of thermally sprayed ceramic coatings," in *Proceedings of the 14th Nordic Insulation Symposium on Materials, Components and Diagnostics*, 2015, pp. 80–85.
[32] M. Niittymäki, T. Suhonen, J. Metsäjoki, and K. Lahti, "Electric field dependency of dielectric behavior of thermally sprayed ceramic coatings," in *Proceedings of the IEEE 11th International Conference on the Properties and Applications of Dielectric Materials (ICPADM)*, 2015, pp. 500–503.
[33] M. Niittymäki, K. Lahti, T. Suhonen, and J. Metsäjoki, "DC conduction and breakdown behavior of thermally sprayed ceramic coatings," *IEEE Trans. Dielectr. Electr. Insul.*, vol. 24, no. 1, pp. 499–510, 2017.
[34] M. Niittymäki, K. Lahti, T. Suhonen, U. Kanerva, and J. Metsäjoki, "Dielectric properties of HVOF sprayed ceramic coatings," in *Proceedings of the IEEE International Conference on Solid Dielectrics*, 2013, pp. 389–392.
[35] E. Turunen *et al.*, "On the role of particle state and deposition procedure on mechanical, tribological and dielectric response of high velocity oxy-fuel sprayed alumina coatings," *Mater. Sci. Eng.* A, vol. 415, no. 1–2, pp. 1–11, Jan. 2006.
[36] C. Neusel, H. Jelitto, and G. A. Schneider, "Electrical conduction mechanism in bulk ceramic insulators at high voltages until dielectric breakdown," *J. Appl. Phys.*, vol. 117, no. 15, p. 154902, 2015.
[37] K.-C. Kao, *Dielectric Phenomena in Solids: With Emphasis on Physical Concepts of Electronic Processes*. Academic Press, 2004.
[38] F. Favre, F. Villieras, Y. Duval, E. Mcrae, and C. Rapin, "Influence of relative humidity on electrical properties of α-Al_2O_3 powders: resistivity and electrochemical impedance spectroscopy," *J. Colloid Interface Sci.*, vol. 286, no. 2, pp. 615–620, 2005.
[39] K. Ahn, B. W. Wessels, and S. Sampath, "Spinel humidity sensors prepared by thermal spray direct writing,", *Sensors Actuators B Chem.*, vol. 107, no. 1, pp. 342–346, 2005.
[40] J. Knuuttila, P. Sorsa, and T. Mäntylä, "Sealing of thermal spray coatings by impregnation," *J. Therm. Spray Technol.*, vol. 8, no. 2, pp. 249–257, Jun. 1999.

Minna Niittymäki (S'13) was born in Sahalahti, Finland, in 1984. She received the M.Sc. degree in electrical engineering from Tampere University of Technology in 2012. Since then she has been working as Researcher in the high voltage research group of the Laboratory of Electrical Energy Engineering at TUT, with the aim towards Ph.D. degree. Her current research interests are in the area of insulation materials focusing on the dielectric characterization of thermally sprayed insulating ceramic coatings.

Kari Lahti (M'01) was born in Hämeenlinna, Finland in 1968. He received the M.Sc. and Doctoral degrees in electrical engineering from Tampere University of Technology in 1994 and 2003, respectively. Since then he has worked at the Laboratory of Electrical Energy Engineering at TUT, currently as a Research Manager and Adjunct Professor. He is the head of TUT's research group on high voltage insulation systems. He has also been responsible for the high voltage laboratory services at TUT since 2002. His research interests are in the area of high voltage engineering including surge arresters, nanocomposite insulation systems, environmental testing of high voltage materials and apparatus, high voltage testing methods and dielectric characterization of insulating materials

Tomi Suhonen was born in Helsinki, Finland, in 1978. He is a Senior Scientist and Manager of multiscale materials modelling activities at VTT Technical Research Centre of Finland. He has 13 years' experience in scientific research related to advanced materials and has published more than 70 scientific papers and holds several international patents.

Jarkko Metsäjoki was born in Rauma, Finland, in 1982. He received M.Sc. degree in materials science from Tampere University of Technology (TUT) in 2008. He has worked at TUT, Braunschweig University of Technology, and since 2012 he has been working at VTT Technical Research Centre of Finland as Research Scientist. He is currently also a PhD student at Aalto University. His research interests include material characterization of thermally sprayed ceramic coatings.